Neuronal control of locomotor handedness in *Drosophila*

Sean M. Buchanan[a], Jamey S. Kain[a], and Benjamin L. de Bivort[a,b,1]

[a]The Rowland Institute at Harvard, Cambridge, MA 02142; and [b]Center for Brain Science and Department of Organismic and Evolutionary Biology, Harvard University, Cambridge, MA 02138

Edited by Ralph J. Greenspan, University of California, San Diego, La Jolla, CA, and accepted by the Editorial Board April 16, 2015 (received for review January 13, 2015)

Genetically identical individuals display variability in their physiology, morphology, and behaviors, even when reared in essentially identical environments, but there is little mechanistic understanding of the basis of such variation. Here, we investigated whether *Drosophila melanogaster* displays individual-to-individual variation in locomotor behaviors. We developed a new high-throughout platform capable of measuring the exploratory behavior of hundreds of individual flies simultaneously. With this approach, we find that, during exploratory walking, individual flies exhibit significant bias in their left vs. right locomotor choices, with some flies being strongly left biased or right biased. This idiosyncrasy was present in all genotypes examined, including wild-derived populations and inbred isogenic laboratory strains. The biases of individual flies persist for their lifetime and are nonheritable: i.e., mating two left-biased individuals does not yield left-biased progeny. This locomotor handedness is uncorrelated with other asymmetries, such as the handedness of gut twisting, leg-length asymmetry, and wing-folding preference. Using transgenics and mutants, we find that the magnitude of locomotor handedness is under the control of columnar neurons within the central complex, a brain region implicated in motor planning and execution. When these neurons are silenced, exploratory laterality increases, with more extreme leftiness and rightiness. This observation intriguingly implies that the brain may be able to dynamically regulate behavioral individuality.

behavior | individuality | personality | circuit mapping | central complex

Hand dominance—better performance using either the left or right hand—is a familiar human trait, moderately heritable (1), and regulated by many genes (2), including those involved in general body symmetry (3). However, behavioral handedness in general, i.e., the preferential performance of a behavior on one side of the body or with a particular chiral twist, is a multifaceted phenomenon. For example, in the absence of visual feedback, people display clockwise or counterclockwise biases in their walking behavior (4). This "locomotor handedness" is uncorrelated to hand dominance or gross morphological asymmetry and instead may be due to asymmetries in the collection and processing of sensory information, resulting in individual locomotor biases with a neurological basis (4, 5).

Handed behavioral tendencies specific to individuals are also prevalent throughout the animal kingdom and have been shown in species as disparate as mice (paw use) (6), octopi (eye use) (7), and tortoises (side rolled on during righting) (8). There is also evidence that, at the population mean level, some species of insects have handed behaviors and asymmetric neurophysiological patterns (9). However, there has been little investigation of the differences in handed behaviors among individuals of the same insect species, and the mechanisms by which asymmetries are instilled in behavior are unknown.

Considering behavioral handedness at the level of individuals offers insight into another major open question in behavioral neuroscience: what is the mechanistic basis of behavioral intragenotypic variability (i.e., the differences in behavior among individuals with the same genotype, reared in identical environments) (10)? There is growing acceptance that individual-to-individual differences in experimental observations of behavior reflect persistent idiosyncrasies (11) rather than just statistical errors, with significant potential impacts on species fitness and ecology (12). Quantifying idiosyncrasy requires large sample sizes, and invertebrate species, with their small size and rapid life cycles, may be particularly valuable (13). Moreover, to probe causal mechanisms underlying idiosyncratic differences in behavior, a paradigm is needed in a molecular model system. We wondered if the fruit fly *Drosophila melanogaster* would exhibit behavioral handedness during exploratory locomotion. If so, the power of high-throughput imaging systems would allow us to automate the quantification of many individuals, opening up the study of idiosyncrasy and behavioral handedness to the powerful screening approaches available in this species.

In flies and other insects, locomotion is under the control of a prominent midline brain structure known as the central complex (in some clades central body). Work from several species has shown that the integration of sensory information and the execution of locomotor patterns are associated with neural activity in these cells (14–17). The central complex consists of four symmetrical neuropils: the protocerebral bridges, the fan shaped body, the ellipsoid body, and the noduli; mutations that disrupt the development of these structures disrupt normal walking behavior (18). Despite substantial insight into processes that depend on the central complex, understanding of the specific neural computations taking place to produce motor outputs is incomplete.

Significance

Genetically identical individuals display variability in their behaviors even when reared in essentially identical environments. This variation underlies both personality and individuality, but there is little mechanistic understanding of how such differences arise. Here, we investigated individual-to-individual variation in locomotor behaviors of fruit flies. Surprisingly, individual flies exhibit significant bias in their left vs. right locomotor choices during exploratory locomotion, with some flies being strongly left biased or right biased. Using the *Drosophila* genetic toolkit, we find that the magnitude of locomotor handedness is under the control of neurons within a brain region implicated in motor planning and execution. This observation intriguingly implies that the brain may be able to dynamically regulate behavioral individuality.

Author contributions: S.M.B., J.S.K., and B.L.d.B. designed research; S.M.B. performed research; S.M.B. and B.L.d.B. analyzed data; and S.M.B., J.S.K., and B.L.d.B. wrote the paper.

The authors declare no conflict of interest.

This article is a PNAS Direct Submission. R.J.G. is a guest editor invited by the Editorial Board.

Freely available online through the PNAS open access option.

[1]To whom correspondence should be addressed. Email: debivort@oeb.harvard.edu.

This article contains supporting information online at www.pnas.org/lookup/suppl/doi:10.1073/pnas.1500804112/-/DCSupplemental.

Here we show that *Drosophila melanogaster* flies exhibit striking locomotor handedness, which varies significantly among individuals. Very strongly biased "lefty" and "righty" individuals are common in every line assayed. The bias of each individual persists for its lifetime. However, mating two lefty flies does not result in lefty progeny, suggesting that mechanisms other than genetics determine individual biases. We use the *Drosophila* transgenic toolkit to map a specific set of neurons within the central complex that regulates the magnitude of locomotor handedness within a line. These findings give insights into choice behaviors and behavioral handedness in a simple model organism and demonstrate that individuals from isogenic populations reared under experimentally identical conditions nevertheless display idiosyncratic behaviors.

Results

Flies Have Idiosyncratic Locomotor Handedness. To investigate whether flies display individual locomotor handedness, we developed a simple high-throughput assay to quantify turning. Flies were placed individually in Y-shaped mazes and allowed to walk freely for 2 h, with their centroids tracked in two dimensions (Fig. 1 *A–C* and Movies S1 and S2). Each maze was symmetrical and evenly lit, so that choices were by design unbiased rather than stimulus driven. The fraction of times the fly passed through the center of the maze and chose to go right defined a turn bias score (Fig. 1*D*). Each fly typically performed hundreds of choices per experiment (Fig. S1*A*). Precise quantification of the distribution of individual behaviors requires large sample sizes, so many mazes were arrayed in parallel (Fig. 1 *A* and *B* and Fig. S1 *B–D*). Thus, our results reflect more than 25,000 individual flies and 16,000,000 turn choices.

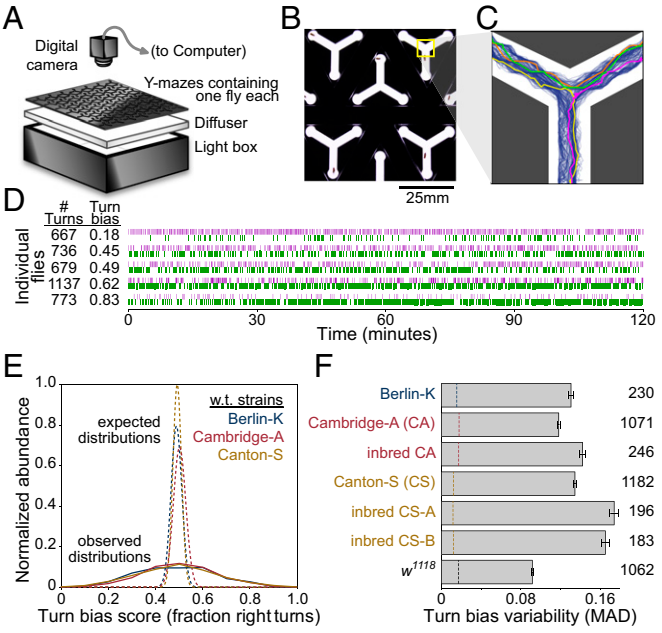

Fig. 1. Individual flies exhibit biases in left-right turning. (*A*) Schematic of a device for assaying left-right turning in individuals. Flies were placed into an array containing many individual Y-mazes. The mazes were illuminated from below and imaged from above, and the positions of the flies were recorded. (*B*) Detail of Y-mazes containing individual flies. (*C*) One hundred example turn paths through the Y-maze recorded from a single fly over 2 h (blue). Other colors highlight individual turns. (*D*) Left and right turn sequences for example flies of varying turn biases. Magenta ticks indicate left turns; green, right. (*E*) Observed distribution of turn bias scores (fraction right turns) measured from WT lines (solid lines), and corresponding expected distributions of turn bias scores (dashed lines). Sample sizes given in *F*. BK, Berlin-K; CA, Cambridge-A; CS, Canton-S. (*F*) The breadth of the distribution of turn bias scores for seven lines as measured by MAD. Error bars are ±SE estimated by bootstrap resampling. Dashed lines indicate MADs expected under a binomial null model. All lines other than w^{1118} (transgenic background line) are nominally WT.

We measured the turn biases of hundreds of individual flies from seven different fly lines: Berlin-K (BK), Canton-S (CS), Cambridge-A (CA) (19), two lines of CS that were independently inbred for 10 generations, CA that was inbred for 10 generations (19), and w^{1118}, the background line for many transgenic flies (Fig. 1 *E* and *F* and Fig. S1*E*). The probability of turning right (the turn bias score), averaged across all individuals within each line was statistically indistinguishable from 50%, an observation that held across all experimental groups. However, this consistency belied profound individual-to-individual variability, and an individual fly's probability of turning right often diverged markedly from the population average. For example, nearly one quarter (23.5%) of CS flies turned right greater than 70% of the time or less than 30% of the time. This distribution would be unlikely indeed if all flies were choosing to turn right with identical probabilities. This null hypothesis can be modeled using the binomial distribution, with each fly performing n_i choices (equal to the number it performed in the experiment) and a probability of turning right p (equal to the mean probability observed across all flies of a given strain). Use of the binomial is statistically justified because sequential turns were essentially independent of one another (Fig. S1*F*). Compared with this null hypothesis, biased righty and lefty individuals are vastly overrepresented ($P < 10^{-16}$ and 10^{-4} by χ^2 test of variance and bootstrap resampling, respectively). To quantify the extent of variation in turn bias, we calculated the mean absolute deviation from the mean (MAD) of individual turn bias scores (Fig. 1*F*). Higher MAD scores indicate greater individual-to-individual differences in behavior, i.e., more extreme left and right biases.

We were unable to identify any trivial sources of left-right turning bias. Neither the light boxes, nor the maze arrays, nor the positions of the mazes within the arrays had any significant effect on the observed mean turning bias (Fig. S1 *B–D*). Anosmic flies (20) displayed the same variability as control flies (Fig. S1*G*), suggesting that flies were not following odor cues within the mazes. Last, activity level did not explain the strong biases of flies; there is no correlation between turn bias score and number of turns completed in the 2-h experiment (Fig. S1*H*).

Individual Locomotor Handedness Is Persistent. Next, we evaluated the persistence of locomotor handedness. Individual flies were tested in the Y-mazes, recovered, stored individually, and then tested a second time, in a different maze, either 1, 2, 6, 13, or 27 d later. Individual turn bias scores were highly correlated across time, ranging from $r = 0.57$ for day 1 vs. day 28 to $r = 0.81$ for day 1 vs. day 2 (all $P < 0.0001$; Fig. 2 *A–D*). The persistence of locomotor handedness through time provides further evidence that biases are not introduced by some experimental artifact. If, for example, flies were following a wall or a trail of odors or pheromones, these results would require that they do so in a highly reproducible manner, over long timescales, and in different Y-mazes.

Locomotor handedness is evidently a persistent property of individual flies—perhaps it reflects a single master regulator of behavioral handedness. We tested this hypothesis by measuring two additional handed behaviors: the direction of spontaneous exploration in circular arenas (Fig. S2) and the folding arrangement of the wings at rest (Fig. S3). We found that individual flies demonstrate a characteristic preference in the direction in which they circle. On average, flies spend equal amounts of time moving clockwise and counterclockwise, but individuals within the population often show strong tendencies to circle in one direction or the other (Fig. S2 *D–F*). Likewise, individual flies exhibit preferences in which wing is placed on top at rest. Some fold left on top of right, others right on top of left (Fig. S3*A*). As with turn

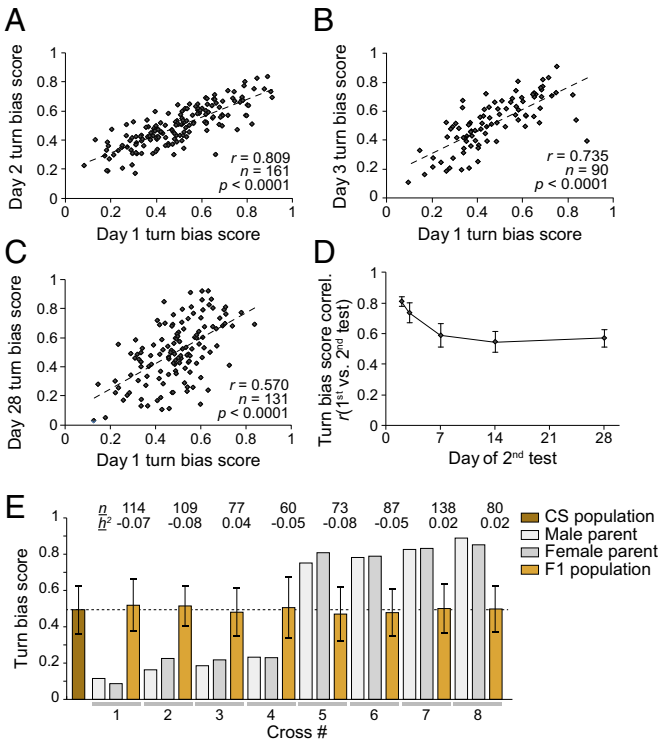

Fig. 2. An individual's handedness is persistent over time. (*A*–*C*) Turn scores from individual flies measured in sequential experiments. Flies were assayed in the Y-mazes, stored individually, and then assayed a second time 1 d (*A*), 2 d (*B*), or 4 wk (*C*) later. (*D*) Correlation coefficient (*r*) of turn bias scores across flies tested in the Y-maze, stored individually, and then tested a second time either 1 d, 2 d, 1 wk, 2 wk, or 4 wk later. Error bars indicate ±SE as estimated by bootstrap resampling. $n = 85$ to $n = 184$ for all time points. (*E*) Mean turn bias of parental (brown) and F_1 generations (tan) derived from strongly biased CS individuals (gray bars). *n* indicates number of F_1s assayed. h^2 indicates estimated heritability. The dashed line indicates 50%. Error bars are ±1 MAD, as a measure of variability rather than error. F_1 and parental distributions are statistically indistinguishable.

bias in the Y-mazes, both arena circling bias and wing-folding bias persist across days (Figs. S2*F* and S3*B*). We tested individual flies in two assays each, maintained their identities, and found that turn bias scores in the Y-maze positively correlate with a clockwise circling bias in the arena (Fig. S2*G*). In contrast, circling bias was completely uncorrelated to wing-folding bias (Fig. S3*C*). From these observations, we conclude that behavioral handedness is multifaceted in *Drosophila*, like humans, but that the turning biases we see in the Y-maze likely reflect an assay-independent locomotor handedness phenomenon.

Genes Tune the Distribution of Locomotor Handedness. There are numerous possible causes of individual turning bias. One potential source of variation is the presence of polymorphic lefty and righty alleles in the population. However, the turn bias of individual flies was not heritable (Fig. 2*E*; mean $h^2 = -0.03$, SE = 0.018, Fisher selection test of heritability) (21), and we found no evidence that inbreeding reduces variability in locomotor bias (Fig. 1*F* and Fig. S1*E*). Although an individual's locomotor handedness is not heritable, the total degree of variability at the population level is under genetic control, with some lines being more variable than others (Fig. 1; CS vs. w^{1118}). The extent of this variation was further confirmed in a companion study of wild-derived inbred lines (22). Another potential source of persistent locomotor handedness is morphological asymmetry. We examined whether variability in leg lengths could account for turning biases. We tested 28 metrics of leg length asymmetry and found that just one correlates with turning bias, and the correlation is weak ($r^2 = 0.11$, $P = 0.007$, $P = 0.18$ after multiple comparisons correction; Fig. S4). Likewise, gut morphological handedness cannot explain locomotor biases because the twist of the gut is identical among individuals (we confirmed this by noting the meconium position in 50 virgin flies).

Given that neither cryptic genetic variation segregating within lines nor morphological asymmetry is a major source of variation in locomotor handedness, perhaps idiosyncratic locomotor asymmetry has a neurobiological basis. The central complex (CC) is a protocerebral structure with integral roles in processing sensory information and controlling locomotor output across arthropods (15, 16, 18, 23, 24). We examined whether disrupting the CC can alter a population's distribution of turn bias scores. First, we tested seven mutants that perturb central complex development and morphology (19). Of these, *no-bridge*, *central-complex-deranged*, and *central-body-defect* (cbd^{KS96}) showed a significant increase in individual variation in turning compared with heterozygous controls (Fig. 3*A*). cbd^{KS96} is a missense mutant of *Ten-a* (25), which encodes a transmembrane protein involved in axon targeting and synapse formation (26, 27), and causes severe and widespread defects in the fan-shaped body (FB), ellipsoid body (EB), and noduli (No), leading to high individual-to-individual variation in the gross morphology of the CC (19). Furthermore, a genome-wide association study in a panel of inbred lines implicated SNPs within *Ten-a* as affecting variability in locomotor handedness (22). This association links natural genetic variation in *Ten-a*, variability in the function of central complex circuits, and variability in turn bias at the population level.

Neural Activity Tunes the Magnitude of Variability in Locomotor Handedness. We next sought to perturb central complex function more specifically with inducible transgenes (28). We selectively silenced different subsets of CC neurons using a panel of *GAL4* lines to express a temperature-sensitive inhibitor of vesicle fusion ($Shibire^{ts}$) (29). By comparing the MADs of the distributions of turn bias scores at the permissive (23 °C) and nonpermissive (33 °C) temperatures, we identified three *GAL4* drivers that regulate the amount of turn bias variability in a population (Figs. 3*B* and 4 and Figs. S5 and S6). Acutely disrupting the function of *c465, R16D01,* or *R73D06* cells by silencing them with $Shibire^{ts}$ caused large increases in the variability of turn bias scores. A similar effect resulted from acutely silencing *c465* cells with $GAL80^{ts}$;*Kir2.1* (24), or by hyperactivating them with *dTRPA1* (30) (Fig. 3*B*).

The *GAL4* lines *c465, R16D01,* and *R73D06* drive expression in subsets of columnar neurons (PFNs) projecting from the protocerebral bridges (PB) to the FB and contralateral No (Figs. 3 *D* and *E* and 4 and Figs. S5, S7, and S8), with dendritic fields in the PB and axonal fields in the FB and No (31, 32) (Fig. 3*E*). *c465* is also expressed in the mushroom bodies, but silencing them had no effect on turn bias variability (Fig. 3*B*). The only cell type present in all three of these lines are the PFNs (Fig. 4 and Figs. S5 and S7). PFNs can be subclassified into one of three types based on the regions of innervation within the FB and No (32). Our data suggest that PFNs projecting to No domain 3 may specifically be the regulators of turn bias variability (Fig. 4 *C* and *D*). Of the six *GAL4* lines in our screen that had PFN expression, the three that had no effect all share strong expression in No domain 4 (Fig. S8), hinting that silencing domain 4 PFNs might counteract or gate the effect of silencing domain 3 PFNs, a possibility that has some statistical support in our data (*Discussion* and *SI Discussion*).

Discussion

We find that *Drosophila* exhibit profound handedness in their locomotor behavior. By developing a high-throughput assay for

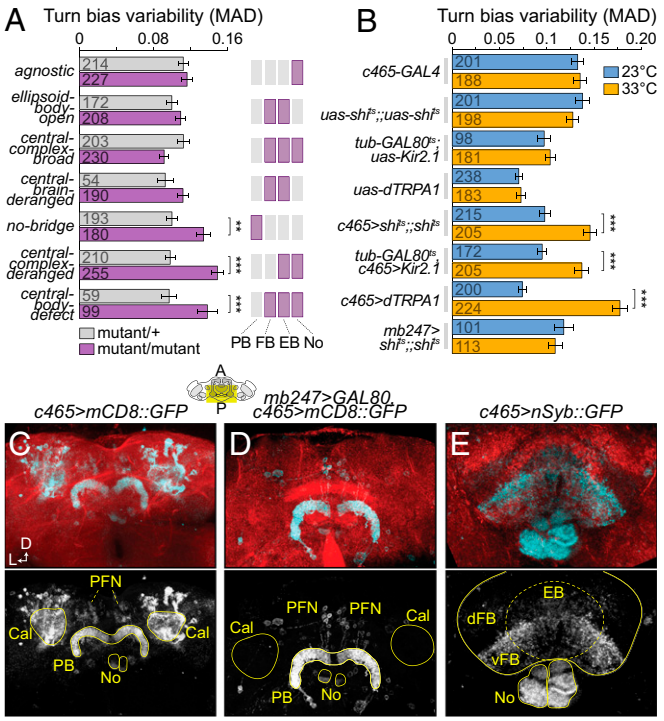

Fig. 3. The central complex regulates variability in turn bias. (*A*) The degree of variability in handedness for seven fly lines carrying mutations that disrupt the development of the central complex (purple bars). Three mutations significantly increase the MAD of the distribution of turn bias scores compared with heterozygous controls (gray bars). $^{**}P < 0.01$, $^{***}P < 0.001$, as estimated by comparing bootstrap resampling of MAD values (15), Bonferroni corrected for multiple comparisons. Error bars are ±SE estimated by bootstrap resampling. Numbers indicate sample sizes. Purple boxes indicate neuropils grossly disrupted by each mutation. (*B*) Turn score variability (MAD) of lines with *c465-GAL4* driving expression of temperature-sensitive modulators of neuronal activity (*GAL80^{ts};Kir2,1*, *Shibire^{ts}*, *dTRPA1*, and control lines) at 23 °C (blue bars) and 33 °C (orange bars) temperatures. Error bars and *P* values as in *A*. (*C–E*) Max fluorescence z-projections of *c465*-driven expression of membrane localized (mCD8) or presynapse localized (nSyb) GFP (cyan), within the central brain (*C*) and central complex (*D* and *E*). Red counterstain is actin. Diagram indicates anterior-posterior extent of z-projection. Cal, mushroom body calyx; PB, protocerebral bridges; No, noduli; EB, ellipsoid body; d/vFB, dorsal/ventral fan-shaped body; PFN, PB-FB-No neurons.

left-right turning, we are able to demonstrate that individual flies show idiosyncratic left-right biases when walking, that strongly left- or right-biased flies are common in the population, and that an individual's locomotor handedness persists throughout its lifetime. This individual-to-individual variation remains in inbred fly populations, is not heritable, and is explained predominantly by factors other than limb morphological asymmetry. Genetic background and mutants affecting the CC, an interconnected group of neuropils involved in the processing of sensory information and the execution of locomotion, can modulate the degree of turn bias variability across individuals. Indeed, the activity level of specific neurons within the central complex alters the breadth of the distribution of turn biases. Our results suggest that genetically and environmentally matched fruit flies exhibit individual differences in the neural processing of sensory information and the execution of locomotor patterns, resulting in profound levels of idiosyncratic locomotor handedness.

Columnar PFNs of the CC may be involved in the integration of bilateral sensory information or the modulation of stimulus signal-to-noise ratios, and asymmetries in their functions may result in asymmetric behavioral outputs. To more rigorously examine this possibility (33), we developed an average firing rate model of a simple left-right decision-making circuit (*SI Discussion* and Fig. S9). This model consists of two input units whose activity reflects the aggregated inputs in favor of left or right turning, respectively. Each input activates one of two outputs that inhibit each other and activate themselves. The activity of these output units determines the motor output—if the left output unit is active, then a left motor instruction is generated and vice versa. Reciprocal inhibition circuits similar to this one have been implicated in sensory signal processing in vertebrates and invertebrates (34, 35). Thus, our purpose here was not to reinvent known circuit models, but rather to rigorously test how, in this established framework, a symmetrical perturbation (e.g., silencing the PFNs) could enhance both left- and right-biased asymmetries.

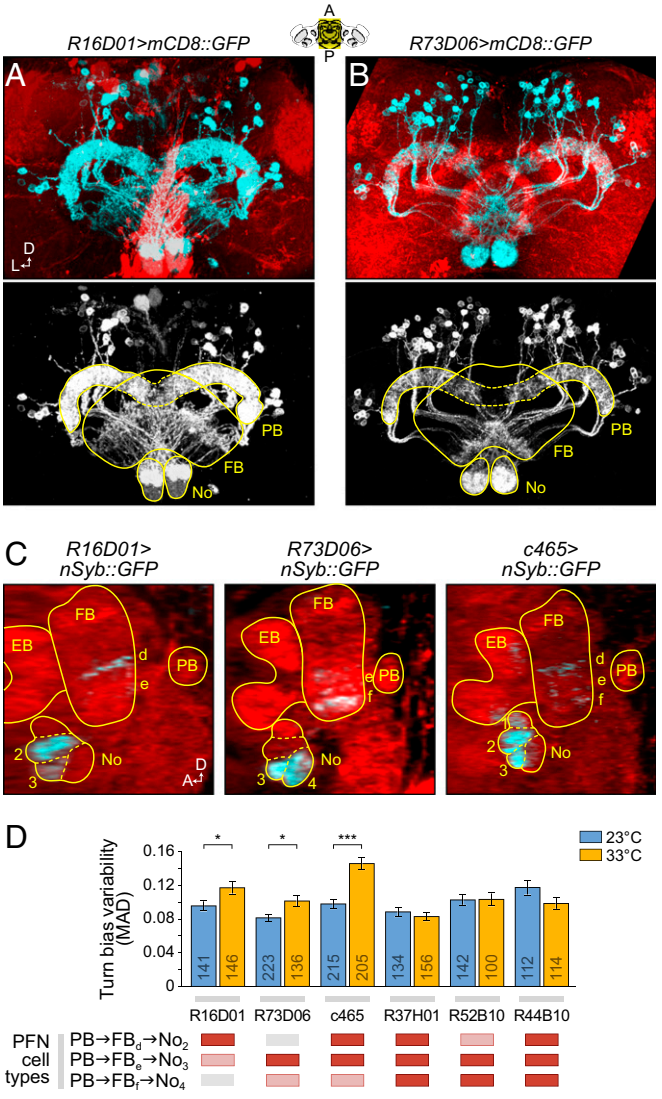

Fig. 4. PFNs regulate variability in turn bias. (*A*) Maximum fluorescence z-projections of *R16D01-GAL4*–driven expression of membrane localized mCD8::GFP (cyan), within the central complex. Red counterstain is actin. Diagram indicates anterior-posterior extent of z-projection. (*B*) As in *A* for the *R73D06-GAL4* driver. (*C*) Lateral views of CD8::GFP driven by *R16D01*, *R73D06*, and *c465-GAL4*. PB, protocerebral bridges; FB, fan-shaped body; No, noduli; EB, ellipsoid body. d, e, f, layers of the ventral fan-shaped body, 1, 2, 3, 4, domains of the noduli. (*D*) Turn score variability of lines with various *GAL4* lines driving shibire at 23 °C (blue bars) and 33 °C (orange bars). Bars are ±SE estimated by bootstrap resampling. Numbers indicate sample sizes. $^{*}P < 0.05$, $^{***}P < 0.001$. Red boxes indicate PFN subtypes with high GAL4 expression; pink boxes indicate lower expression.

Our model assumes that a network of reciprocal inhibitory connections amplify differences in inputs, resulting in a winner-takes-all output. Such an inhibitory network may be present in GABAergic EB neurons. Upstream neuropils of the EB within the CC include the FB and the PB, implicating the *c465* neurons as inputs to the decision-making circuit. In our model, we found that circuit perturbations that increase the signal-to-noise-ratio of the inputs evoking choice behavior result in an increase in behavioral variability by increasing the relative importance of any small network asymmetry inherent to an individual. Conversely, when the signal-to-noise ratio is reduced, noise begins to dominate, and every individual behaves more like a fair coin, thus reducing variability. No other perturbation had this effect. Thus, a reasonable hypothesis for the effects we observed is that silencing the PFNs increases the signal-to-noise ratio in the stimuli driving locomotor choice behavior.

How might silencing PFNs increase the signal-to-noise ratio of inputs driving left-right decisions? Activity in the protocerebral bridges may encode information useful for turning decision making in circumstances other than the experimental setting of our Y-mazes. Indeed, visual information flows via at least two routes to the CC: from the polarized light-sensitive dorsal rim ommatidia to the protocerebral bridges (17) and from the higher-order feature detectors of the optic lobe and optic glomeruli to the lateral triangle (and EB) (36). Because there are no polarized light sources in our experiment, it is plausible that activity in *c465* neurons constitutes noise with respect to useful visual stimuli. Because presynapses of *c465* neurons are found in the ventral FB and No, these neuropils may be the sites at which stimuli relevant and irrelevant for locomotor turn decision making are integrated. This framework may also shed light on our observation that both silencing *c465* neurons (with Shibire^{ts}) and increasing their activity (with dTRPA1) increased variability. Both of these manipulations have the potential to "peg" neural activity in a regime that cannot encode any information. Although Shibire^{ts} increased variability, neither Kir2.1 nor dTRPA1 had an effect when driven by *R16D01* and *R73D06*. These *GAL4* lines appear to have lower expression than *c465*, so perhaps they did not drive these effectors strongly enough to peg neural activity and block information transmission.

Our intersectional analysis suggests that the role of PFNs in regulating locomotor handedness may vary between PFN subtypes. Lines with the strongest expression in PFNs projecting to the third domain of the noduli had the greatest effect on turn bias variability, whereas those with expression in the fourth domain had the least effect. There may be a gating or additive relationship between the PFN subtypes, such that silencing PFNs projecting to domain 3 of the noduli increases turn bias variability, but simultaneously silencing PFNs projecting to domain 4 blocks or counters the domain 3 effect. This scenario has some statistical support (*SI Discussion*). The development of GAL4 lines specific to these subtypes will allow us to rigorously test such hypotheses.

Locomotor handedness has been observed in humans (4, 5). In these studies, subjects were asked to walk in a straight line in the absence of visual feedback, a task that proved difficult and resulted in subjects veering off course and circling. Testing across multiple trials revealed a spectrum of consistency, with some subjects always veering left, some always veering right, and others showing inconsistent biases. An individual's circling bias correlated to asymmetries in their posture, which in turn is based on the integration of neural inputs and the internal representation of their body's position in space. Individual asymmetries in the collection and processing of information from the vestibular, proprioceptive, and other sensory systems may therefore result in inherent biases in locomotor behaviors. There are obvious parallels between these results and our findings in flies. Fly locomotor handedness manifests itself as either a bias in left-right turning, or a propensity to turn clockwise or counterclockwise in an arena, and we demonstrate a clear role for brain regions implicated in the integration of multiple sensory inputs.

Just as locomotor handedness, hand clasping, arm folding, and hand dominance are all independent in humans (37), we found that fly locomotor handedness and wing folding are uncorrelated. It remains an appealing research direction to determine whether flies exhibit preferential left vs. right limb use in tasks requiring dexterity. One paradigm that could be illuminating is gap crossing (38, 39) in which flies walk along a raised platform and, by first extending their forelegs, are able to cross gaps wider than their body length. Notably, columnar neurons in the PB are required for coordinated gap crossing. Perhaps flies exhibit a consistent preference in which foreleg they lead with. Using an instrument that rapidly tracks the position of each leg, we previously observed that individual flies show persistent idiosyncrasies in their limb positioning during the transitions between behavioral states like postural adjustment and walking (40). Thus, it is plausible that they exhibit an equivalent of hand dominance.

We and others have shown that genetically and environmentally similar individuals can develop idiosyncratic behaviors, morphology, and gene expression profiles. For example, stochastic DNA methylation may contribute to phenotypic variation that is uncorrelated to genetic variation (41). Stochastic gene expression may underlie the phenomenon of partial penetrance of mutations and variability in the escape responses of the nematode *Caenorhabditis elegans* (42). Morphologically, invertebrates can display a remarkable degree of individual variation in the development of neural connectivity (43, 44). For example, a detailed anatomical study of lobula descending neurons (LDNs) (45), a pair of cells that project from the optic lobes to the ventral nerve cord in several species of insect, revealed that these cells can have highly variable dendritic morphologies. Strikingly, some flies have more than twice as many LDN dendritic spines on one side of the brain compared with the other, and one individual displayed 29 postsynaptic dendritic branches in the left lobula plate but none in the right. These types of stochastic differences in neuronal morphology may be common across the nervous system.

In addition to variable morphology, individuals with identical genotypes and raised in identical environments can display variable behaviors. Genetically identical offspring of the facultatively asexual aphid *Acyrthosiphon pisum* display surprising variability in their predator avoidance behaviors, a phenomenon that may help the aphid population escape a variety of insectivores (46). Similarly, a quantitative analysis of locomotion in *Aphis fabae*, another clonal aphid, suggested that individual insects display idiosyncrasy in their food-foraging behaviors (47). In *Drosophila*, WT siblings display idiosyncratic preferences when given the choice of two odors (48). Work in our laboratory has shown that inbred flies reared identically show broad diversity in their phototactic behavior and the extent of this variation is under the control of serotonin (19). Individual variation in both wiring and behavior may prove to be a very general feature of neural circuits.

Taken together, our results suggest that when a fly must make a left vs. right decision in the absence of an asymmetric stimulus, asymmetries within the brain predispose the animal to go one way rather than the other and that neural activity influences the degree of variation between animals. Perhaps it is a feature of noisy biological systems that allows the animal to avoid detrimental inaction when presented with ambivalent stimuli. In either case, brain asymmetry is implicated in psychiatric disorders (49), suggesting that regulation of individual-to-individual variability may have clinical dimensions. Individual variation in wiring (44, 45, 50), physiology (51), and behavior (19, 40) may prove to be a very general feature of neural circuits, with broad implications both for our basic understanding of developmental

neurobiology and the emergence of behavioral phenotypes at the individual level.

Materials and Methods

See *SI Materials and Methods* for details. All raw data, data acquisition software, and analysis scripts are available at lab.debivort.org/neuronal-control-of-locomotor-handedness/.

Fly Care. Flies were housed on modified Cal Tech medium according to standard protocols. A full list of the lines used in this study is available in Table S1. Flies used for *Shibire^{ts}* experiments were reared at 25 °C and transferred to 23 or 33 °C 30 min before and during data collection. *GAL80^{ts};Kir2.1* experimental groups were reared at 18 °C, transferred to 30 °C for 48 h before testing, and transferred to 33 °C for data collection; controls were kept at 18 °C until testing at 33 °C.

Behavior. Four- to 8-d-old flies were placed into individual Y-mazes or arenas and allowed to walk freely for 2 h. Mazes were illuminated from below with white LEDs (5,500 K; LuminousFilm) and imaged with 2-MP digital cameras (Logitech; Point Gray), and the X-Y positions of the flies' centroids were automatically tracked using background subtraction and recorded with software custom written in LabView (National Instruments). Data were then analyzed with custom written scripts in MatLab (The MathWorks). Data from flies making fewer than 50 turns were discarded. For day-to-day experiments, identity was maintained by storing flies individually in labeled culture vials between tests.

Statistics and Modeling. All statistical calculations were done in MatLab. Expected turn bias distributions (Fig. 1*E* and Fig. S1*E*) were calculated by summing binomial distributions with n_i equal to the number of choices made by fly i within the corresponding experimental group, and p_i equal to the average right turn probability of the entire population. P values determined by bootstrapping are reported as 95% CI upper bounds. P values were Bonferroni corrected for multiple comparisons as appropriate. Model simulations (Fig. S9) were performed in MatLab (The MathWorks) using Euler approximation.

ACKNOWLEDGMENTS. We thank Mike Burns, Chris Stokes, and other members of The Rowland Institute for fruitful scientific discussions and technical assistance, as well as Julien Ayroles, Kit Longden, Frank Hirth, Tom Maniatis, Charles Zuker, and members of their laboratories for helpful feedback. We thank Shmuel Raz, Roland Strauss, Michael Reiser, Aravi Samuel, Sam Kunes, Chuntao Dan, Douglas Armstrong, and Hiromu Tanimoto for sharing fly lines. We thank the Janelia Farm FlyLight consortium for allowing us to reuse and modify their *GAL4* expression images. This research was funded in part by the Junior Fellows Program at The Rowland Institute at Harvard.

1. Medland SE, et al. (2009) Genetic influences on handedness: Data from 25,732 Australian and Dutch twin families. *Neuropsychologia* 47(2):330–337.
2. McManus IC, Davison A, Armour JA (2013) Multilocus genetic models of handedness closely resemble single-locus models in explaining family data and are compatible with genome-wide association studies. *Ann N Y Acad Sci* 1288:48–58.
3. Brandler WM, et al. (2013) Common variants in left/right asymmetry genes and pathways are associated with relative hand skill. *PLoS Genet* 9(9):e1003751.
4. Souman JL, Frissen I, Sreenivasa MN, Ernst MO (2009) Walking straight into circles. *Curr Biol* 19(18):1538–1542.
5. Bestaven E, Guillaud E, Cazalets J-R (2012) Is "circling" behavior in humans related to postural asymmetry? *PLoS ONE* 7(9):e43861.
6. Collins RL (1968) On the inheritance of handedness. I. Laterality in inbred mice. *J Hered* 59(1):9–12.
7. Byrne RA, Kuba MJ, Meisel DV (2004) Lateralized eye use in *Octopus vulgaris* shows antisymmetrical distribution. *Anim Behav* 68(5):1107–1114.
8. Stancher G, Clara E, Regolin L, Vallortigara G (2006) Lateralized righting behavior in the tortoise (*Testudo hermanni*). *Behav Brain Res* 173(2):315–319.
9. Frasnelli E (2013) Brain and behavioral lateralization in invertebrates. *Front Psychol* 4:939.
10. Stamps JA, Saltz JB, Krishnan VV (2013) Genotypic differences in behavioural entropy: Unpredictable genotypes are composed of unpredictable individuals. *Anim Behav* 86(3):641–649.
11. Sih A, Bell AM, Johnson JC, Ziemba RE (2004) Behavioral syndromes: An intergrative overiew. *Q Rev Biol* 79(3):241–277.
12. Dall SRX, Houston AI, McNamara JM (2004) The behavioral ecology of personality: Consistent individual differences from an adaptive perspective. *Ecol Lett* 7(8):734–739.
13. Kralj-Fiser S, Schuett W (2014) Studying personality in invertebrates: Why bother? *Anim Behav* 91:41–52.
14. Bender JA, Pollack AJ, Ritzmann RE (2010) Neural activity in the central complex of the insect brain is linked to locomotor changes. *Curr Biol* 20(10):921–926.
15. Liu G, et al. (2006) Distinct memory traces for two visual features in the *Drosophila* brain. *Nature* 439(7076):551–556.
16. Ritzmann RE, Ridgel AL, Pollack AJ (2008) Multi-unit recording of antennal mechanosensitive units in the central complex of the cockroach, *Blaberus discoidalis*. *J Comp Physiol A Neuroethol Sens Neural Behav Physiol* 194(4):341–360.
17. Vitzthum H, Muller M, Homberg U (2002) Neurons of the central complex of the locust *Schistocerca gregaria* are sensitive to polarized light. *J Neurosci* 22(3):1114–1125.
18. Strauss R, Heisenberg M (1993) A higher control center of locomotor behavior in the *Drosophila* brain. *J Neurosci* 13(5):1852–1861.
19. Kain JS, Stokes C, de Bivort BL (2012) Phototactic personality in fruit flies and its suppression by serotonin and white. *Proc Natl Acad Sci USA* 109(48):19834–19839.
20. Larsson MC, et al. (2004) Or83b encodes a broadly expressed odorant receptor essential for *Drosophila* olfaction. *Neuron* 43(5):703–714.
21. Fisher RA (1918) The correlation between relatives on the supposition of Mendelian inheritance. *Trans R Soc Edinb* 52:399–433.
22. Ayroles JF, et al. (2015) Behavioral idiosyncracy reveals genetic control of phenotypic variability. *Proc Natl Acad Sci USA*, 10.1073/pnas.1503830112.
23. Strauss R (2002) The central complex and the genetic dissection of locomotor behaviour. *Curr Opin Neurobiol* 12(6):633–638.
24. Ofstad TA, Zuker CS, Reiser MB (2011) Visual place learning in *Drosophila* melanogaster. *Nature* 474(7350):204–207.
25. Cheng X, et al. (2013) Ten-a affects the fusion of central complex primordia in *Drosophila*. *PLoS ONE* 8(2):e57129.
26. Hong W, Mosca TJ, Luo L (2012) Teneurins instruct synaptic partner matching in an olfactory map. *Nature* 484(7393):201–207.
27. Mosca TJ, Hong W, Dani VS, Favaloro V, Luo L (2012) Trans-synaptic Teneurin signalling in neuromuscular synapse organization and target choice. *Nature* 484(7393):237–241.
28. Brand AH, Perrimon N (1993) Targeted gene expression as a means of altering cell fates and generating dominant phenotypes. *Development* 118(2):401–415.
29. Kitamoto T (2001) Conditional modification of behavior in *Drosophila* by targeted expression of a temperature-sensitive shibire allele in defined neurons. *J Neurobiol* 47(2):81–92.
30. Hamada FN, et al. (2008) An internal thermal sensor controlling temperature preference in *Drosophila*. *Nature* 454(7201):217–220.
31. Young JM, Armstrong JD (2010) Structure of the adult central complex in *Drosophila*: Organization of distinct neuronal subsets. *J Comp Neurol* 518(9):1500–1524.
32. Lin CY, et al. (2013) A comprehensive wiring diagram of the protocerebral bridge for visual information processing in the *Drosophila* brain. *Cell Reports* 3(5):1739–1753.
33. Servedio MR, et al. (2014) Not just a theory—the utility of mathematical models in evolutionary biology. *PLoS Biol* 12(12):e1002017.
34. Olsen SR, Wilson RI (2008) Lateral presynaptic inhibition mediates gain control in an olfactory circuit. *Nature* 452(7190):956–960.
35. Yokoi M, Mori K, Nakanishi S (1995) Refinement of odor molecule tuning by dendrodendritic synaptic inhibition in the olfactory bulb. *Proc Natl Acad Sci USA* 92(8):3371–3375.
36. Mota T, Yamagata N, Giurfa M, Gronenberg W, Sandoz JC (2011) Neural organization and visual processing in the anterior optic tubercle of the honeybee brain. *J Neurosci* 31(32):11443–11456.
37. McManus IC, Mascie-Taylor CGN (1979) Hand-clasping and arm-folding: A review and a genetic model. *Ann Hum Biol* 6(6):527–558.
38. Pick S, Strauss R (2005) Goal-driven behavioral adaptations in gap-climbing *Drosophila*. *Curr Biol* 15(16):1473–1478.
39. Triphan T, Poeck B, Neuser K, Strauss R (2010) Visual targeting of motor actions in climbing *Drosophila*. *Curr Biol* 20(7):663–668.
40. Kain J, et al. (2013) Leg-tracking and automated behavioural classification in *Drosophila*. *Nat Commun* 4:1910.
41. Lukens LN, Zhan S (2007) The plant genome's methylation status and response to stress: Implications for plant improvement. *Curr Opin Plant Biol* 10(3):317–322.
42. Topalidou I, Chalfie M (2011) Shared gene expression in distinct neurons expressing common selector genes. *Proc Natl Acad Sci USA* 108(48):19258–19263.
43. Bucher D, Prinz AA, Marder E (2005) Animal-to-animal variability in motor pattern production in adults and during growth. *J Neurosci* 25(7):1611–1619.
44. Chou YH, et al. (2010) Diversity and wiring variability of olfactory local interneurons in the *Drosophila* antennal lobe. *Nat Neurosci* 13(4):439–449.
45. Nässel DR, Strausfeld NJ (1982) A pair of descending neurons with dendrites in the optic lobes projecting directly to thoracic ganglia of dipterous insects. *Cell Tissue Res* 226(2):355–362.
46. Schuett W, et al. (2011) Personality variation in a clonal insect: The pea aphid, *Acyrthosiphon pisum*. *Dev Psychobiol* 53(6):631–640.
47. Petrovskii S, Mashanova A, Jansen VA (2011) Variation in individual walking behavior creates the impression of a Levy flight. *Proc Natl Acad Sci USA* 108(21):8704–8707.
48. Claridge-Chang A, et al. (2009) Writing memories with light-addressable reinforcement circuitry. *Cell* 139(2):405–415.
49. Klar AJS (2004) An epigenetic hypothesis for human brain laterality, handedness, and psychosis development. *Cold Spring Harb Symp Quant Biol* 69:499–506.
50. Caron SJ, Ruta V, Abbott LF, Axel R (2013) Random convergence of olfactory inputs in the *Drosophila* mushroom body. *Nature* 497(7447):113–117.
51. Sakurai A, Tamvacakis AN, Katz PS (2014) Hidden synaptic differences in a neural circuit underlie differential behavioral susceptibility to a neural injury. *eLife* 3:e02598.

Supporting Information

Buchanan et al. 10.1073/pnas.1500804112

SI Materials and Methods

Fly Care. Fly lines were grown on standard modified Cal Tech medium in vials stored in temperature-controlled incubators. Humidity was maintained using water pans at ∼40% relative humidity. Incubators were lit on a 12-h/12-h light-dark cycle using LED illuminators. On a daily basis, flies were collected out of stock tubes and kept in cohorts of 15–60 in fresh vials for 4–7 d, assuring that all animals tested were 4–8 d old.

Maze Fabrication. Mazes were cut into 1/16-in.-thick black acrylic using a laser engraver (Epilog). Each arm of a maze was 0.37 in. long and 0.13 in. wide. To inhibit the flies from flipping upside down, the floors of the mazes were lightly roughened with a random orbital sander and fine-grit sand paper, and clear acrylic lids (one per maze) were lubricated with Sigmacote (Sigma). Circular arenas were fabricated similarly and were 2 in. in diameter. A diffuser made of two sheets of 1/4-in.-thick clear acrylic roughened on both sides by orbital sanding, placed between the LED array and the maze array, provided for uniform illumination.

Circling Bias Estimation. In calculating circling biases (in circular arenas), centroids were tracked, and the direction of fly motion was inferred as the angle between the centroids of successive frames. Flies were scored as moving if their centroids changed by more than 0.5 px per frame. Typically, the size of the region of interest spanning one circular arena was 80 × 80 px. To avoid edge artifacts, all path segments farther from the center of the arena than 80% of the radius were ignored, although this made little qualitative difference.

Wing Folding. To measure the wing-folding preference of individual flies, we moved each fly into a vial singly. The vial was flicked or agitated until the fly flew, assuring that its wings were unfolded. We then anesthetized it with CO_2 and examined it manually under a dissecting scope to determine which wing was on top. The animal was then returned to its vial and allowed to waken, at which point we repeated the process. Flies were examined in this way five times sequentially per day. To generate the day-to-day correlation (Fig. S3*B*), we compared the aggregated wing-folding data from days 1 and 2 (10 total observations) with the aggregated data from days 3 and 4 (another 10 total observations). Similarly, the flies that were first measured for wing folding and then turning bias in the Y-maze were scored for the former over 2 d (10 total observations) and tested in the Y-maze on day 3.

Leg Measurement. Flies that had first been measured in the Y-maze were stored individually in vials, anesthetized, and dissected. Each leg was removed between the middle and base of the coxa. Legs and the body were placed flat on a backing of double-sided tape on a microscope slide. Images were acquired using a digital camera on a tripod, and leg segment and body lengths were determined digitally in ImageJ in units of pixels.

Statistics. In determining expected turn bias distributions, a null hypothesis binomial distribution was calculated for each fly in the experiment. These individual curves were interpolated into a normalized [0,1] domain before being summed and renormalized for comparison against observed distributions. MAD was chosen as our metric for variability because it is well characterized, nonparametric, and weights data points equally. (Standard deviation, by contrast, weighs outlying points more heavily.) SEs of MAD scores and correlation coefficients were calculated using bootstrap resampling, with a minimum of 1,000 replicates.

P values based on bootstrap resampling were used in three different ways. (*i*) To compare observed MADs to known null hypotheses (Fig. 1 *E* and *F*), samples were drawn from the known null distribution in numbers corresponding to the data. The number of samples in which the MAD of the randomly drawn values equal or was less than that of the null hypothesis was recorded. If the bootstrap replicates produced the tested condition by chance alone at a rate of k out of n resamples, p was reported as the highest probability such that CDF[binomial(n, p), k] > 0.025. That is, the highest value of p that would yield the tested event k times out of n or fewer at least 2.5% of the time. (*ii*) To compute bootstrapped z-tests (Fig. S5*B*), we determined the number of SEs away from 0 the observed MAD was by bootstrapping the points contributing to that MAD value. (*iii*) To compare the MADs of two experimental groups (Figs. 3 *A* and *B* and 4*D* and Fig. S6), we assumed the bootstrap-estimated errors on the MADs were Gaussian and calculated the one-tailed probabilities of that a MAD drawn from the experimental error distribution would be less than a MAD drawn from the control error distribution. Mutual information (Fig. S1*F*) was calculated on a fly-by-fly basis between turn t and $t + 1$. Significance asterisks in Fig. 3*A* reflect a Bonferroni correction for multiple comparisons. Significance in Figs. 3*B* and 4*D* is not corrected because comparisons are only between 23 °C and 33 °C experimental groups.

Immunohistochemistry and Imaging. Adult nervous tissue was dissected and fixed overnight in 4% paraformaldehyde at 4 °C. After fixation, tissue was counterstained with Alexa Fluor 568 conjugated to phalloidin for 24–48 h (Life Technologies; 1:50 dilution). Stained brains were washed in phosphate-buffered saline with Tween 20 (PBT) and mounted on glass slides in 70% glycerol or vectaShield mounting medium (Vector Labs). Images were collected on a Zeiss LSM710 or LSM780 confocal microscope. Panels modified from FlyLight images (Figs. S7 *D–F*, *Right*, and S8, bottom row) were downloaded from flweb.janelia.org/cgi-bin/flew.cgi and color rotated into a red-cyan palette. Depth-coded images (Fig. S7*F*) and lateral views (Fig. 4*C* and Fig. S8) were calculated using stack functions in FIJI (fiji.sc/Fiji).

Modeling. Runs of the average firing rate model (Fig. S9) were computed in MATLAB using custom scripts implementing the Euler approximation, with $\Delta t = 0.01$. The model was considered converged (i.e., a decision had been made) if variables changed by less than 0.001 between iterations, or at 1,000 iterations, whichever was earlier. Tuning curves were determined empirically based on 1,000 replicates of the model. Behavioral distributions were based on 1,000 tuning curves. The β fitting parameters were determined analytically from the means and variances of the behavioral distributions. Additional model description is provided in *SI Discussion*. The model was highly robust to parameter choice, and the parameter values used for Fig. S9 are $\alpha_L = \alpha_R = 0.01$, $\beta_L = \beta_R = 0.02$, $\delta = 0.03$, $\gamma_R = 0.01$, and $\gamma_L = 0.01b$, where b determines the intrinsic network bias. Stimulus noise was implemented as $L'_{in}(0) = L_{in}(0) + \varepsilon_1$ and $L'_{in}(0) = L_{in}(0) + \varepsilon_2$, where $\varepsilon_i \sim N(\mu,\sigma^2)$, with $\mu = 0$ in all cases, $\sigma = 0.1$ for the green curves, and $\sigma = 0.2$ for the purple curves of Fig. S9. Intrinsic bias was normally distributed with mean = 1 and SD = 0.025 in Fig. S9*C* and 0.01 in Fig. S9 *D* and *E*.

SI Discussion

Statistical Support for Differential Effects of PFN Subtypes. Three *GAL4* lines with expression in the PFNs modify the variability of turn bias scores when perturbed transgenically (*c465*, *R73D06*, and

R16D01). Our screen (Fig. S5) also contained three lines (*R37H01*, *R52B10*, and *R44B10*) with expression in PFNs, which had no effect (Fig. 4*D*). Although these lines may have had no effect for all of the usual experimental reasons, e.g., not driving *Shibire*^{ts} strongly enough or not being expressed in a sufficient number of PFNs, we saw some indications that the lines that had no effect shared aspects of their expression patterns (Fig. 4*D*). Specifically, these lines all had strong expression in domains 4 (and 3) of the noduli. Perhaps the effect of silencing PFNs is dose dependent, so that silencing an intermediate number of PFNs, or all PFNs at an intermediate level, results in modulation of turn bias score variability, whereas silencing them all or very strongly undoes the effect.

Alternatively, as described in *Discussion*, there may be PFN subtype-specific effects on locomotor handedness variability. Perhaps silencing PFNs projecting to domain 3 of the noduli increases variability, whereas silencing PFNs projecting to domain 4 decreases variability. The true test of this hypothesis will come with the construction of GAL4 reagents specific to each of these subtypes.

In the meantime, even though the number of available independent *GAL4* lines is low, we did conduct a simple statistical test of the idea that silencing domain 3 PFNs increases variability, whereas silencing domain 4 PFNs reduces it. Specifically, we used the expression coding from Fig. 4*D* (*Lower*) and fit a linear model where the fold change in MAD from permissive to restrictive temperatures of a particular *GAL4* line = a*D2 + b*D3 + c*D4, where a, b, and c, were fit based on the observed data, and D2, D3, and D4 represent the relative level of expression in that *GAL4* line in noduli domains 2, 3, and 4, respectively, coded as 0 if there was no detectable expression, 1 for weak or intermediate expression, and 2 for strong expression. These steps were repeated 10,000 times in each of which (*i*) the data from individual flies in each experimental group were resampled with replacement and (*ii*) the *GAL4* lines (out of the six) were also resampled with replacement. For each repetition, the linear coefficients a, b, and c, were fit as above. Any resampled trials in which three or fewer *GAL4* lines were chosen were overdetermined and rejected.

Across these bootstrap replicates, the mean fold change in MAD was estimated to be −0.052 when silencing noduli domain 2 neurons (a), 0.51 when silencing domain 3 (b), and −0.49 when silencing domain 4 (c). The 95% CI values of a, b, and c were estimated as (−0.51, 0.28), (0, 1.29), and (−1.0, 0), respectively. The mean r^2 on the linear fit was 0.58 and $P = 0.047$. Thus, there is some statistical support for the notion that silencing PFNs projecting to domain 4 may reduce turn bias score variability, whereas silencing PFNs projecting to domain 3 increases variability. Definitive tests of this hypothesis will be possible when new genetic reagents allow us to target specific PFN subtypes.

A Model of Asymmetry and Noise in Left-Right Decision Making. We were curious how a symmetrical perturbation (e.g., silencing the PFNs) could enhance both left- and right-biased asymmetries. To investigate this, we explored a general decision-making circuit model and found that circuit perturbations that decrease the signal-to-noise ratio of the stimuli triggering choice behavior result in an increase in behavioral variability by increasing the relative importance of any small inherent network asymmetry. We found no other perturbation that had this effect. Thus, a reasonable hypothesis for the effects we observed is that silencing the PFNs increases the signal-to-noise ratio in the stimuli driving locomotor choice behavior. Our purpose here was not to reinvent known models of reciprocal inhibition but rather to rigorously test our intuition that a plausible explanation of the effects of silencing PFNs is through a modulation of stimulus signal-to-noise ratios.

It is striking that perturbation of these neurons results in the exacerbation of asymmetric locomotor behaviors in a way that affects left and right bias equivalently. The overall symmetry of the distribution of turn bias scores is maintained, suggesting that any minor asymmetries in this expression pattern are incidental to its symmetric effect on the frequency of left- and right-biased animals. Likewise, it is unlikely that the effect of silencing the PFNs is due to consistent asymmetry in their structure (compare the asymmetric body) (1), as silencing or hyperactivating an asymmetrical circuit in a background of symmetrical behaviors would likely introduce asymmetry detectable in the average behavior.

To explore circuit dynamics that might underlie these observations, we implemented the average firing rate model described in the main text and shown in Fig. S9. Over a wide range of parameters, this circuit amplifies any difference between left and right stimuli and produces a pattern of all-or-none left vs. right output (Fig. S9*B*). This lack of variability is, of course, biologically implausible. Even in strongly stimulus-evoked behaviors, animals exhibit a variety of behavioral outcomes. This trial-to-trial stochasticity can be built into the model by adding a random error term to the initial stimulus representations (L_{in} and R_{in}; Fig. S9*B*). This addition reshapes the stimulus-locomotor tuning curve from an idealized square wave to a more plausible sigmoidal shape. That is, when the input stimuli are strongly biased, the output behavior approaches 100% left or 100% right turns, but when stimuli are ambiguous, arbitrary left-right behavioral probabilities can be attained.

In our Y-maze experiments, animals were presented with essentially identical, highly ambivalent stimuli. There were no systematic cues to drive the animals left or right. Nevertheless, flies exhibited a broad distribution of left-right turning biases. In the framework of our model, this observation can be recreated by introducing processing asymmetries across individuals (Fig. S9 *C* and *D*). In one implementation, we varied according to a normal distribution the ratio of the strengths of the reciprocal inhibitory connections between the output units. This variation resulted in a population of tuning curves and consequently a broad distribution of left-right behavioral outcomes induced by ambiguous stimuli. Tuning the variance in processing asymmetry has a direct effect on the breadth of the behavioral distribution (which in all cases was well fit by a β function; Fig. S9 *D* and *E*). The latter distribution corresponds to the entire population of flies with its diverse collection of turn bias scores. Thus, the amount of locomotor variation specific to each strain can be accounted for by a particular amount of individual-to-individual variation in neural substrates, either in their physiology or wiring.

With the circuit model now reflecting levels of behavioral variability specific to each line, we can investigate manipulations that broaden or narrow the behavioral distribution while holding constant the magnitude of interanimal network asymmetries. Many symmetrical manipulations, such as proportionally scaling the strengths of the reciprocal inhibitory connections (or self-activating connections or activating connections from input to output units), have no effect. However, modulating the input signal-to-noise ratio by adding Gaussian noise to L_{in} and R_{in} profoundly affects the breadth of the behavioral distribution (Fig. S9*E*). Interestingly, decreasing the signal-to-noise ratio narrows the behavioral distribution and flattens the population of sigmoidal tuning curves as they pass through the regime of ambivalent stimuli. In other words, decreasing the salience of whatever stimuli induce the animals to turn either left or right causes random stimulus-encoding error to dominate behavior, rather than endogenous bias. Across many trials, this will drive behavior toward its mean across animals, narrowing the distribution of behaviors.

1. Pascual A, Huang KL, Neveu J, Préat T (2004) Neuroanatomy: Brain asymmetry and long-term memory. *Nature* 427(6975):605–606.

2. Kain JS, Stokes C, de Bivort BL (2012) Phototactic personality in fruit flies and its suppression by serotonin and white. *Proc Natl Acad Sci USA* 109(48):19834–19839.

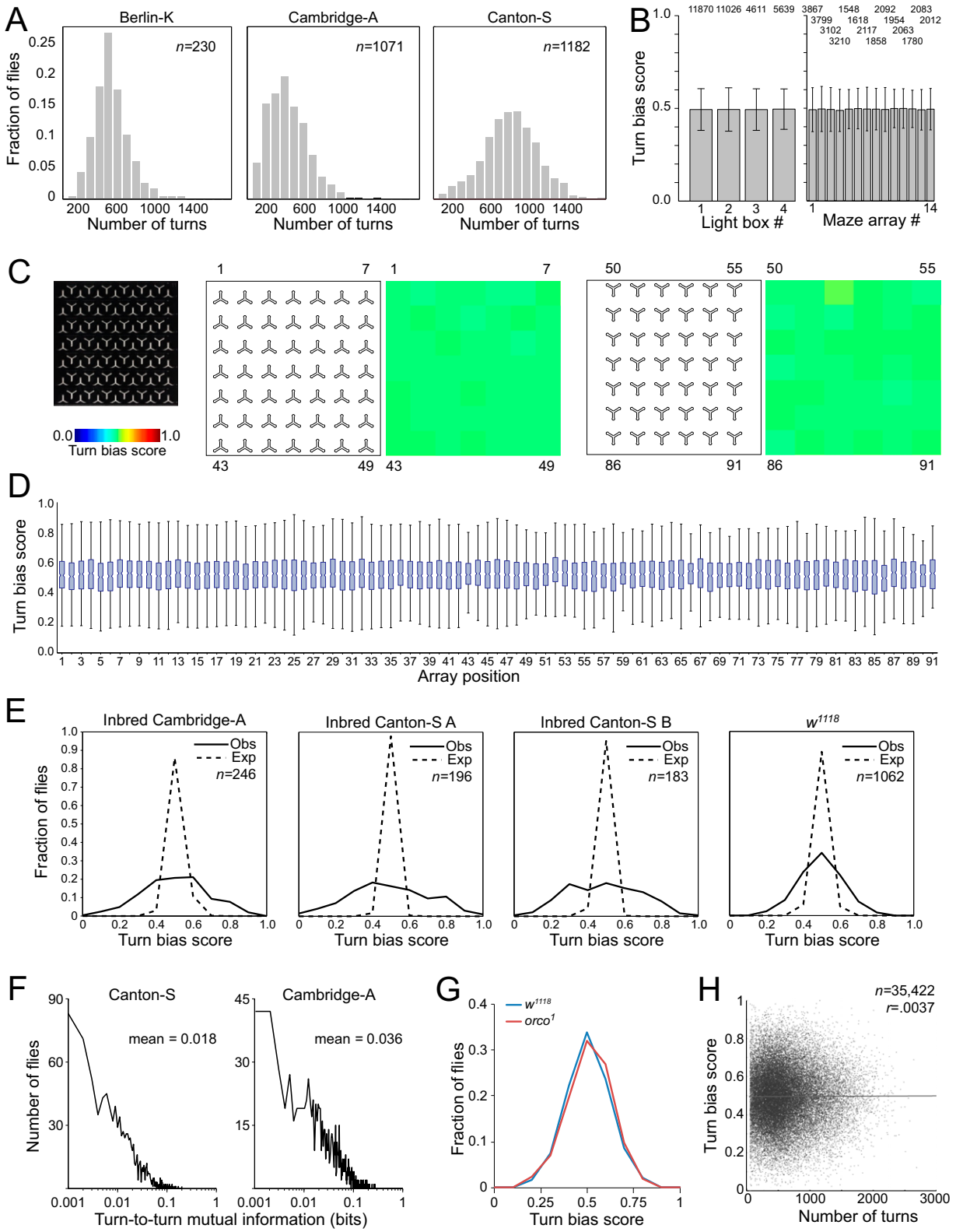

Fig. S1. Y-maze assay performance and controls. (*A*) The distribution of the total number of turns completed in 2 h for three WT lines. (*B*) Experiments were carried out with 14 different maze arrays containing grids of either 49, 91, or 120 individual mazes and imaged on four light box and camera imaging rigs. (*Left*) Average turn bias score ± MAD for all flies assayed in each of the four light box and camera setups. Numbers indicate sample sizes. (*Right*) Average turn bias score ± MAD for all flies assayed in each of the 14 arrays of Y-mazes. (*C*) Example photograph of an array of 91 mazes (*Left*). Average turn bias score for all flies in each of the first 49 maze array positions (center-left diagram and heat map), and for mazes in positions 50–91 (right diagram and heat map). Green in heat maps indicates mean turn bias scores of 0.5. Statistics of 120 maze arrays are similar. (*D*) One-way ANOVA analysis of all flies run at each position in the 91

Legend continued on following page

maze arrays. No position has a significantly different distribution of turn bias scores; $P = 0.450$. Waist of box plot indicates median turn bias score. Box edges indicate 25th and 75th percentiles. Whiskers indicate range excluding outliers. Statistics of 120 maze arrays are similar. (*E*) The distribution of observed (solid lines) and expected (dotted lines) turn bias scores for four WT fly lines. (*F*) Fly-by-fly distributions of the mutual information between successive turns in the Y-maze for two WT lines. Mutual information equal to 1 denotes complete dependence of each turn on the previous turn; 0 is complete independence. (*G*) Olfactory input does not alter the distribution of turn bias scores. The distribution of turn bias scores was determined for a broad spectrum olfactory mutant (*orco*^{1}, $n = 212$) and the corresponding background line (*w*^{1118}, $n = 1{,}062$). (*H*) The number of completed turns does not correlate to turn bias score.

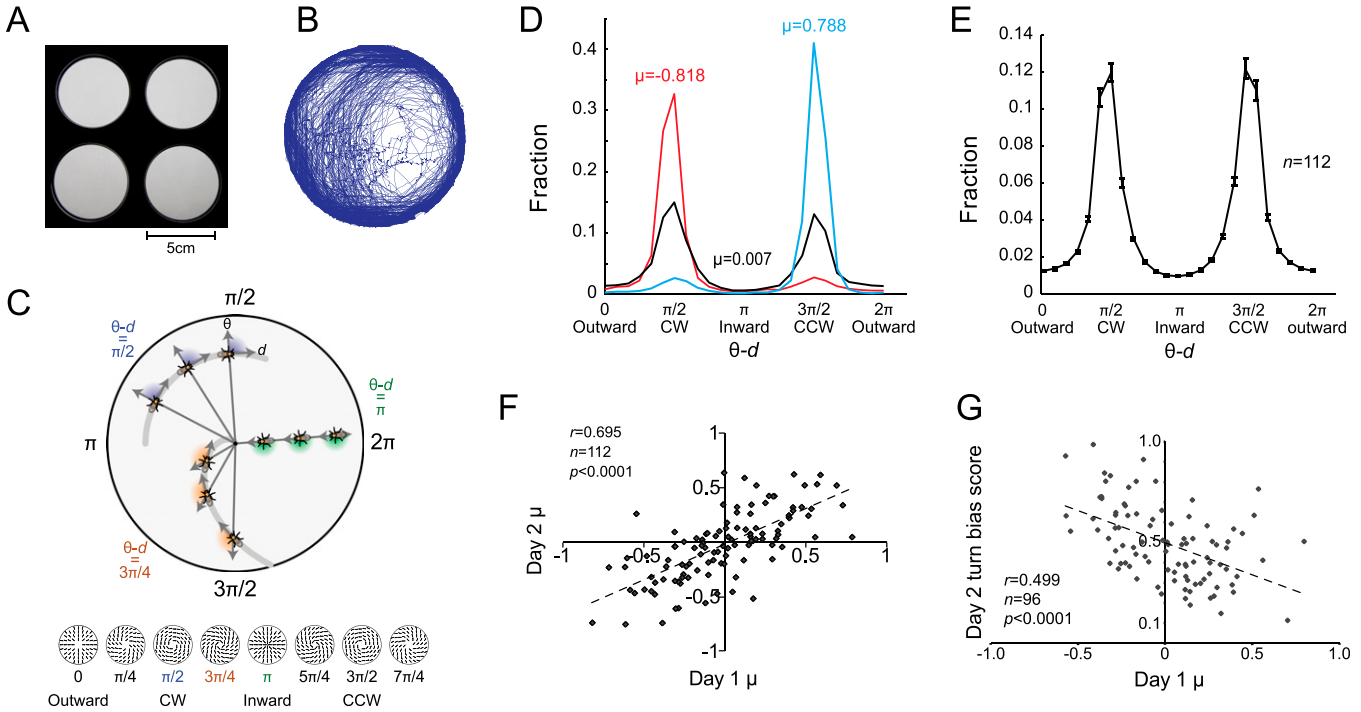

Fig. S2. Individual flies exhibit circling bias in an open arena. (*A*) An open arena assay for exploratory locomotion. Individual flies were placed in circular arenas and allowed to walk freely for 2 h, and their position was tracked as in Fig. 1. (*B*) Example path data collected from a single fly over 2 h. (*C*) For each data point, a circling score is calculated by subtracting the fly's direction of motion (d) from its angular position (θ) in radians. This gives the circumferential component of motion, with π/2 indicating clockwise motion (CW), 3π/2 indicating counterclockwise motion (CCW), 0 indicating walking straight into the center of the arena, and π indicating walking straight out from the center. (*D* and *E*) Histograms of circling scores for a strongly CW-biased individual, a CCW-biased individual, and a relatively unbiased individual (*D*), and the average circling of 112 flies (*E*). (*F*) Measures of average circling are correlated between testing days across flies. μ is the averaged signed circumferential component of motion (vel_{circum}/speed); 1 corresponds to purely CCW motion, −1 corresponds to purely CW motion, and 0 corresponds to equal (or no) CW and CCW motion. (*G*) Circling bias scores (μ) as measured in the arena are correlated to turn bias scores as measured in the Y-maze. Flies were assayed in the open arenas, stored individually, and then assayed 24 h later in the Y-mazes.

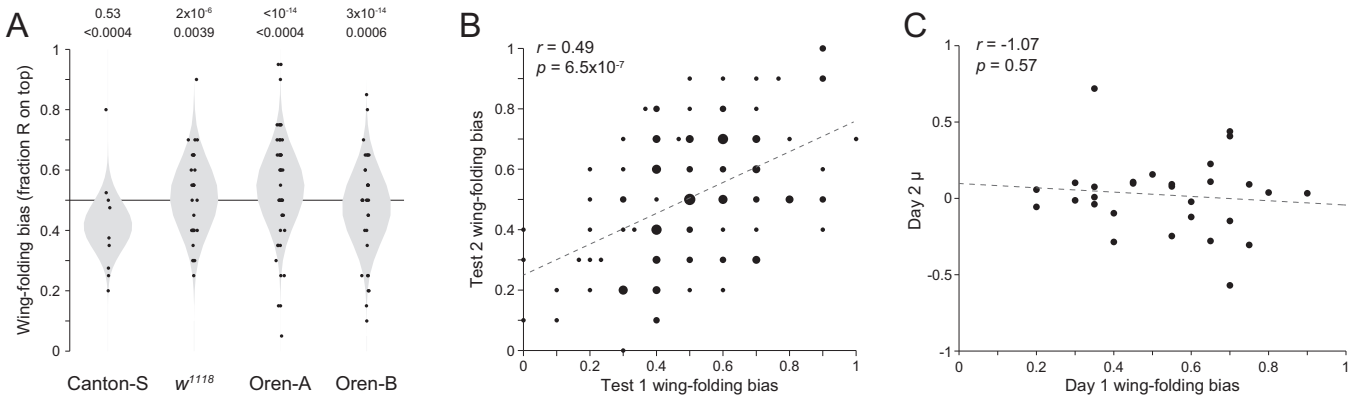

Fig. S3. Individual flies exhibit wing-folding bias. (*A*) Wing-folding bias scores (points) for individual flies. Gray distributions reflect null hypotheses based on the number of times each fly was assessed and the mean observed across all flies. Top row of *P* values are from the χ^2 test of variance, bottom row from bootstrap resampling. (*B*) Bubble plot of wing-folding scores over subsequent days of testing (days 3 and 4 vs. 1 and 2; *Materials and Methods*). The areas of points reflect the number of superimposed data points. Data are aggregated from the four lines shown in *A*; the same positive trend was present in all lines individually. (*C*) Scatter plot of arena circling bias score (μ) vs. wing-folding score for individual flies measured in both assays and whose identities were preserved by single housing.

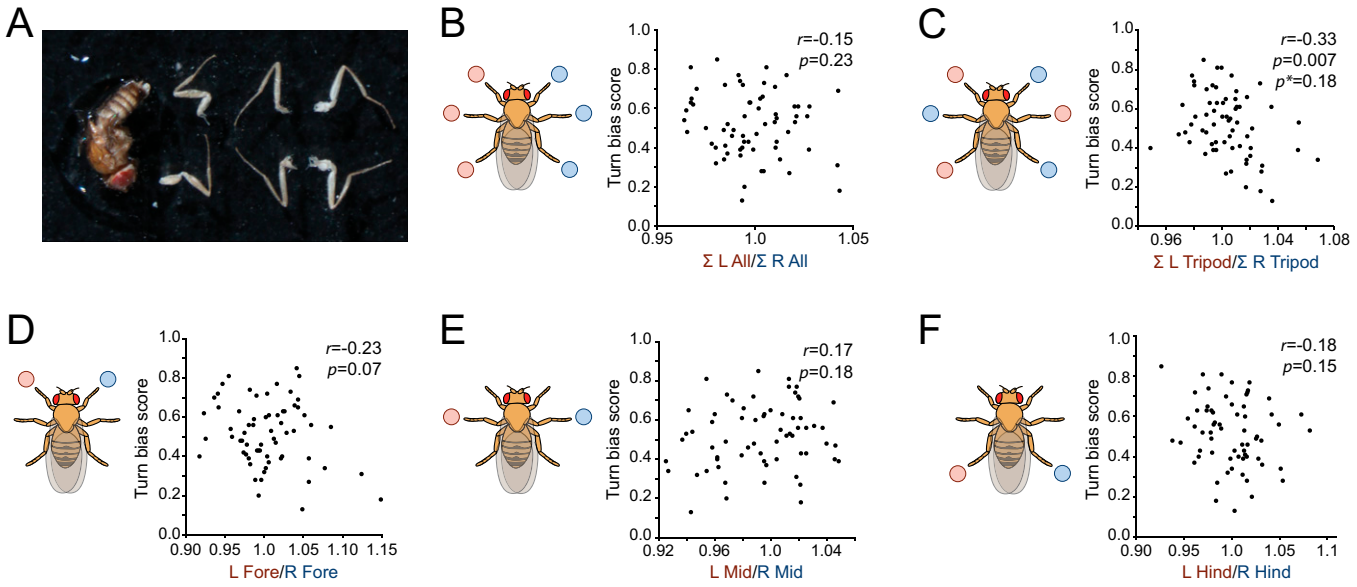

Fig. S4. The contribution of leg morphology to handedness. (*A*) Sixty-five flies were assayed in the Y-maze and preserved in 100% ethanol. Legs were removed and photographed, and the lengths of the leg femurs, tibia, and tarsi were measured, along with the length of the body. Shown is a representative preparation for measurement. (*B–F*) Scatter plots where each point represents an individual's turn bias score vs. the ratio of (*B*) total length of left legs vs. total length of right legs, (*C*) total length of the left tripod vs. right tripod, (*D*) left foreleg vs. right foreleg, (*E*) left midleg vs. right midleg, and (*F*) left hindleg vs. right hindleg. Twenty-three other correlations between turn bias score and individual leg or segment length were also considered, so the Bonferroni correction for multiple comparisons in *C*, *p**, reflects that number of comparisons.

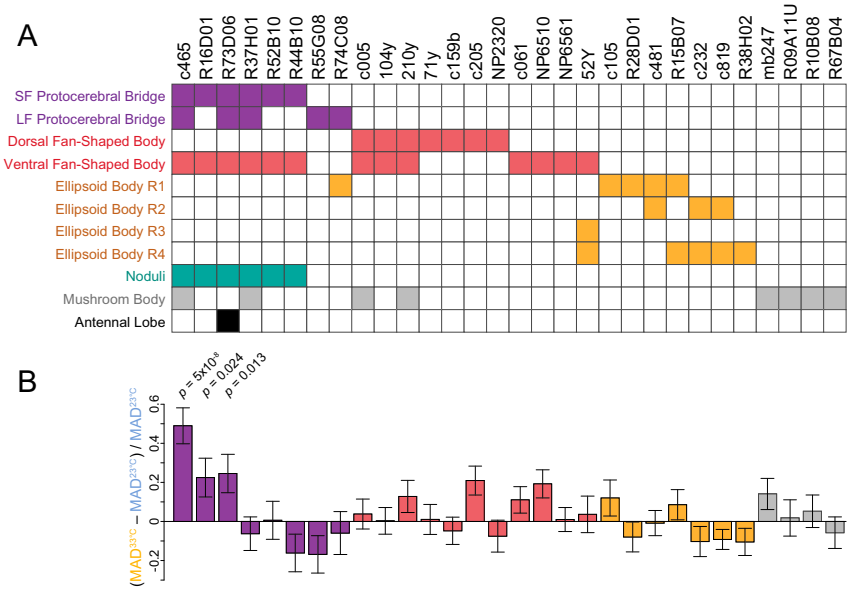

Fig. S5. A screen of *GAL4* lines for neurons affecting handedness. (*A* and *B*) Thirty different sparsely expressed *GAL4* lines were used to drive temperature-sensitive *Shibire* in subsets of central complex (and other brain regions). Colored cells in table (*A*) indicate regions of expression. (*B*) For each line, % difference in the variability of turn bias scores (ΔMAD/MAD) between the restrictive (33 °C) and permissive (23 °C) temperatures. Error bars indicate error estimated by bootstrap resampling. *P* values for the three lines with effects (top rows) were determined by a *z*-test on the number of SEs between the estimate of the % MAD difference and 0.

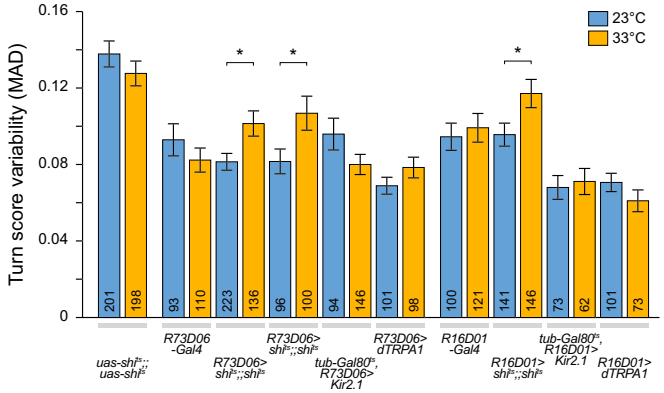

Fig. S6. PFN GAL4 lines regulating handedness. Turn bias score variability (MAD) of lines with either *R73D06* or *R16D01-GAL4* driving expression of temperature sensitive modulators of neuronal activity (*GAL80^{ts};Kir2,1*, *Shibire^{ts}*, *dTRPA1*, and control lines) at 23 °C (blue bars) and 33 °C (orange bars) temperatures. Unlike *c465-GAL4*, these drivers had no effect when driving *Kir2.1* or *dTRPA1*; their baseline effect sizes were also lower. Column pairs 3 and 4 represent two separate *R73D06* > *Shibire^{ts}* conducted a few weeks apart. Bars are ±SE estimated by bootstrap resampling. Numbers indicate sample sizes.

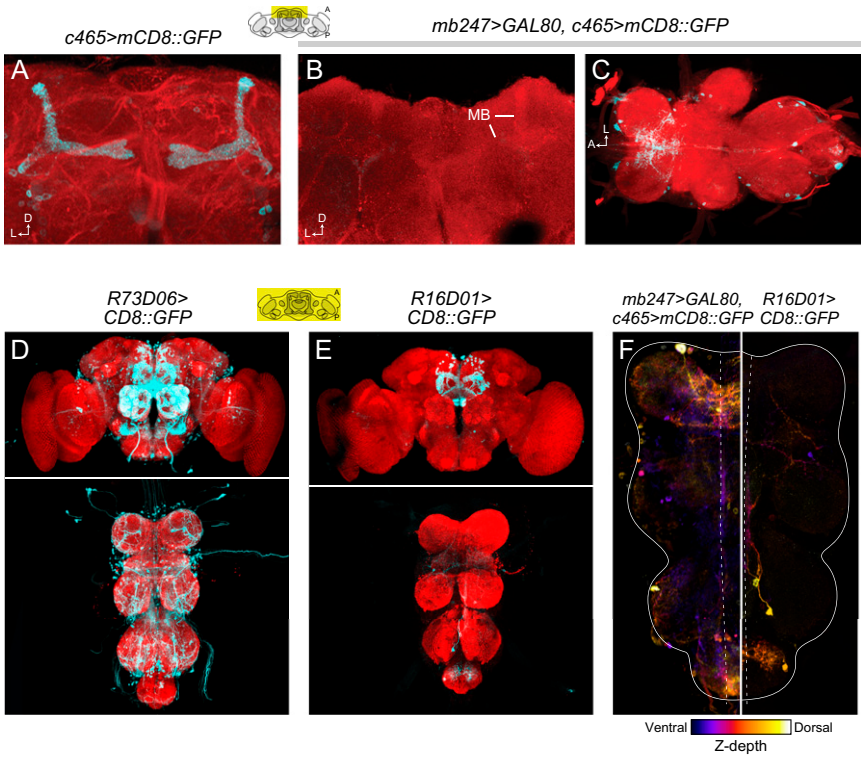

Fig. S7. GAL4 expression pattern analysis. (*A*) Maximum fluorescence z-projection of *c465*-driven expression of CD8::GFP (cyan) within the central brain. Red counterstain is actin. Diagram indicates anterior-posterior extent of z-projection in *A* and *B*. (*B*) Projection as in *A* in a fly with *c465-GAL4* and *MB247-GAL80* driving CD8::GFP expression. All staining in the mushroom bodies (MB) is eliminated. (*C*) Maximum projection through the entire A-P axis of the ventral nerve cord (VNC), same genotype as *B*. (*D*) Maximum projections through the entire brain (*Upper*) and VNC (*Lower*) of CD8::GFP driven by *R73D06-GAL4*. (*E*) As in *D* for the driver *R16D01-GAL4*. (*F*) Depth-coded image of CD8::GFP expression as driven by *c465-GAL4;MB247-GAL80* (*Left*) and *R16D01* (*Right*). There are no cells common to both expression patterns within the VNC. Images in *D–F* (*Right*) were reproduced and modified with permission from published FlyLight translation stacks (flweb.janelia.org/cgi-bin/flew.cgi).

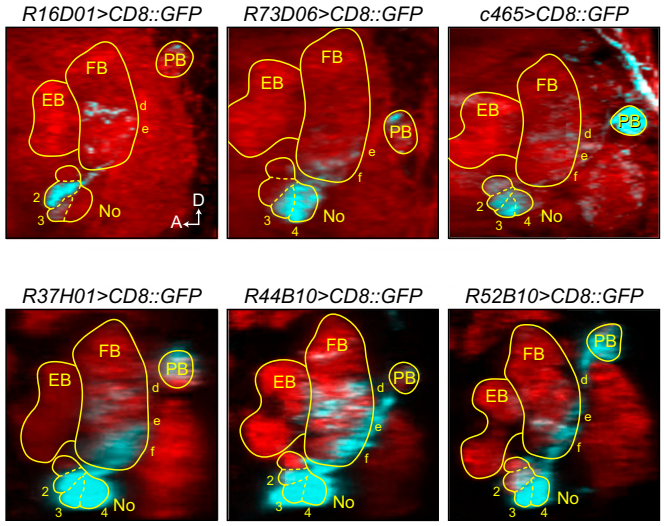

Fig. S8. PFN subtype analysis. Single slice lateral views through the central complex reconstructed from confocal stacks. On the medial-lateral axis, slices are centered on the noduli. CD8::GFP driven by labeled *GAL4* drivers (cyan). Red counterstain in the top row is actin and anti-nc82 staining in the bottom row. PB, protocerebral bridges; FB, fan-shaped body; No, noduli; EB, ellipsoid body. d, e, f, layers of the ventral fan-shaped body; 1, 2, 3, 4, domains of the noduli. Images in the bottom row reproduced and modified with permission published from FlyLight translation stacks (flweb.janelia.org/cgi-bin/flew.cgi).

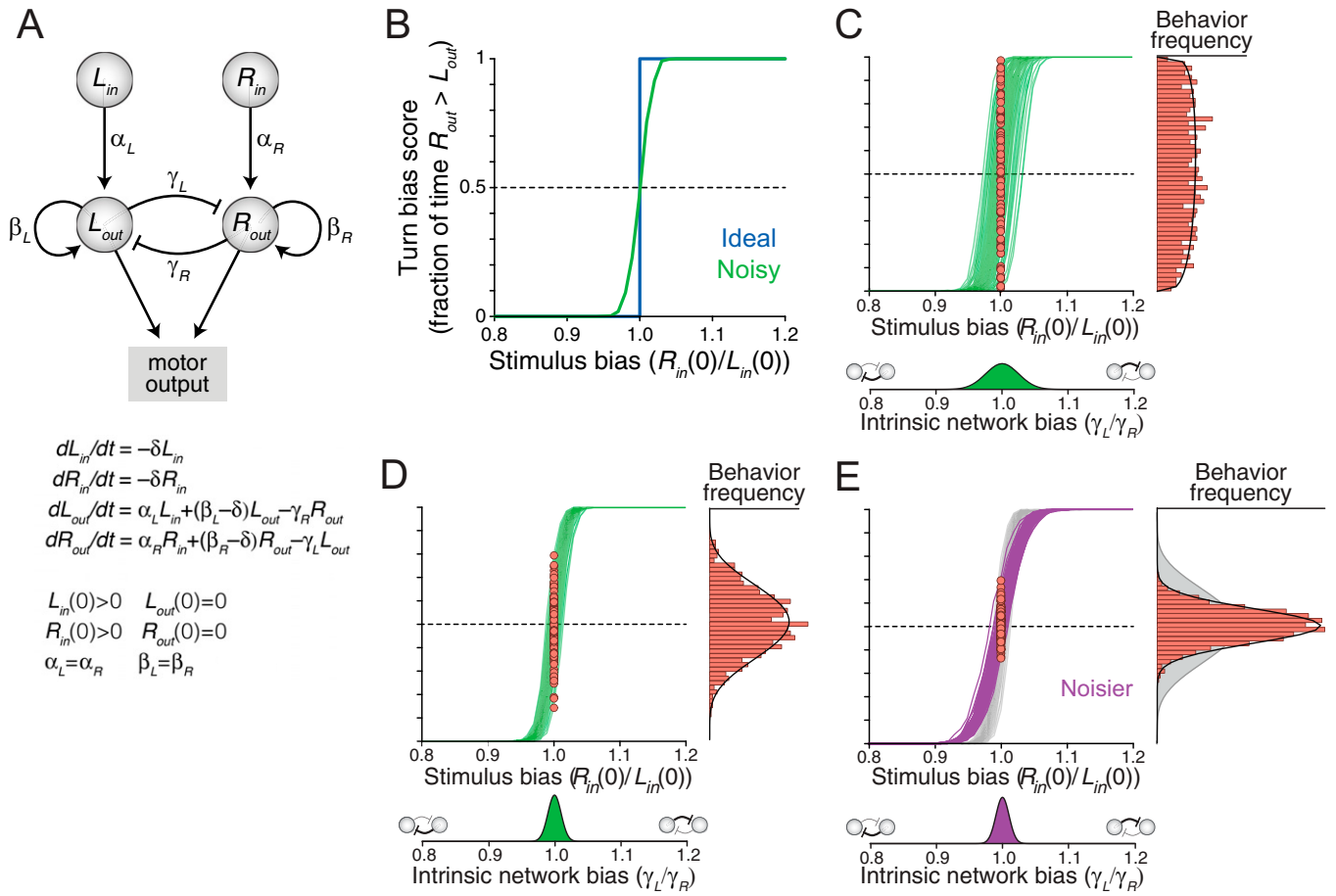

Fig. S9. A model of idiosyncrasy in locomotor decision making. (*A*) Mutual-inhibition model of a decision-making circuit. Activity in L_{in} and R_{in} represents the summed stimuli favoring left and right turning, respectively. These nodes activate L_{out} and R_{out} (with strengths α_L and α_R), which are reciprocally inhibitory with strengths γ_L and γ_R. After the model state has converged, motor behavioral output is scored as left if $L_{out} > R_{out}$ and vice versa. Terms of the model, initial conditions, and assumptions are given in the *SI Materials and Methods* and *SI Discussion*. (*B*) The model generates ideal decisions in the absence of noise (i.e., any small bias in stimulus results in a complete motor bias). Introducing Gaussian noise to the stimulus results in a more plausible sigmoidal stimulus-locomotor tuning curve. See *Materials and Methods* and *SI Discussion* for details. (*C*) Introducing individual-to-individual variation in the intrinsic bias of the network (e.g., by skewing the ratio of reciprocal inhibitory strengths γ_L and γ_R) results in individuals exhibiting a variety of left-right biases under identical stimulus circumstances (red points, which are binned into a histogram at right). *y* axes as in *B*; fit (black line) is provided by a β function. (*D*) Reducing individual-to-individual network asymmetry reduces behavioral variability compared with *C*. (*E*) Decreasing the stimulus signal-to-noise ratio flattens the stimulus-locomotor tuning curve and reduces variability in behavioral outcomes. Gray data are from *D* and are shown for comparison.

Table S1. Strains used in this study and their origins

Strain	Source
Berlin-K	BSC #8522
Cambridge-A	Laboratory stocks (2)
Cambridge-A iso	Laboratory stocks (2)
Canton-S	W. Quinn (MIT)
Canton-S isoA	This work
Canton-S isoB	This work
white^{1118}	J. Dubnau (CSHL)
Oren-A	S. Raz (IEUH)
Oren-B	S. Raz (IEUH)
agnostic^{X1}	R. Strauss (JGUM)
central-body-defect^{KS96}	R. Strauss (JGUM)
central-brain-deranged^{849}	R. Strauss (JGUM)
central-complex-broad^{KS145}	R. Strauss (JGUM)
central-complex-deranged^{KS135}	R. Strauss (JGUM)
ellipsoid-body-open^{678}	R. Strauss (JGUM)
no-bridge^{KS49}	R. Strauss (JGUM)
orco^{1}	BSC #23129
UAS-dTRPA1	BSC #26263
tubP-Gal80^{ts};UAS-Kir2.1	M. Reiser (JFRC)
UAS-mCD8-GFP	BSC #5136
UAS-nSyb-GFP	S. Kunes (HU)
UAS-Shibire^{ts};;UAS-Shibire^{ts}	C. Dan (JFRC)
52y-GAL4	D. Armstrong (UE)
71y-GAL4	D. Armstrong (UE)
104y-GAL4	D. Armstrong (UE)
210y-GAL4	D. Armstrong (UE)
c005-GAL4	D. Armstrong (UE)
c061-GAL4	D. Armstrong (UE)
c105-GAL4	D. Armstrong (UE)
c159b-GAL4	D. Armstrong (UE)
c205-GAL4	D. Armstrong (UE)
c232-GAL4	D. Armstrong (UE)
c465-GAL4	D. Armstrong (UE)
c481-GAL4	D. Armstrong (UE)
c819-GAL4	D. Armstrong (UE)
mb247-GAL4	S. Kunes (HU)
mb247-GAL80	H. Tanimoto (MPIN)
NP2320-GAL4	DGRC #104157
NP6510-GAL4	DGRC #113956
NP6561-GAL4	DGRC #105258
R09A11U-GAL4	M. Reiser (JFRC)
R10B08-GAL4	M. Reiser (JFRC)
R15B07-GAL4	M. Reiser (JFRC)
R16D01-GAL4	M. Reiser (JFRC)
R28D01-GAL4	M. Reiser (JFRC)
R38H02-GAL4	M. Reiser (JFRC)
R67B04-GAL4	M. Reiser (JFRC)
R73D06-GAL4	M. Reiser (JFRC)

All stocks originally supplied by M. Reiser (JFRC) are now available from BSC. BSC, Bloomington Stock Center; CSHL, Cold Spring Harbor Laboratory; DGRC, *Drosophila* Genetic Resource Center; HU, Harvard University; IEUH, Institute of Evolution, University of Haifa; JFRC, Janelia Farm Research Campus; JGUM, Johannes-Gutenberg Universitaet Mainz; MIT, Massachusetts Institute of Technology; MPIN, Max Planck Institute for Neurobiology; UE, University of Edinburgh.

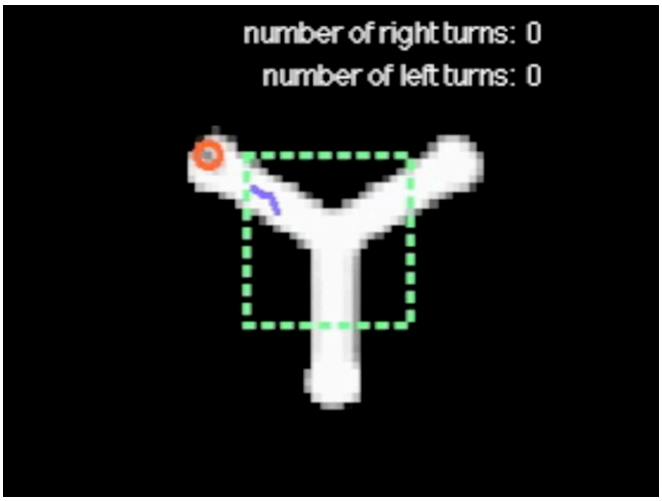

Movie S1. A Y-maze locomotor choice assay. A movie demonstrating a single fly exploring a Y-maze for 2 min. As the fly passes through the center of the maze (green box) its centroid is tracked (red circle) and its path is recorded (blue lines). Passes through the choice point are scored as left or right turns in post processing.

Movie S1

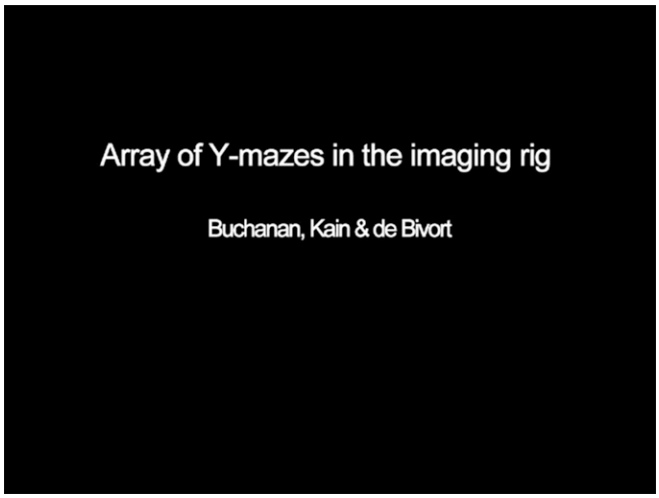

Movie S2. An array of Y-mazes in the imaging rig. A movie demonstrating 91 individual flies simultaneously exploring separate Y-mazes. Each array of 91 mazes was constructed out of laser cut acrylic, evenly illuminated from below with diffuse white light, and imaged from above.

Movie S2